Phase separation in structural and magnetic transitions in $Pr_{0.5}Ca_{0.5-x}Sr_xMnO_3$ (x = 0.15 and 0.3)

2001 J. Phys.: Condens. Matter 13 6813

(http://iopscience.iop.org/0953-8984/13/31/317)

INSTITUTE OF PHYSICS PUBLISHING JOURNAL OF PHYSICS: CONDENSED MATTER

J. Phys.: Condens. Matter **13** (2001) 6813–6834 PII: S0953-8984(01)21604-X

Phase separation in structural and magnetic transitions in $Pr_{0.5}Ca_{0.5-x}Sr_xMnO_3$ (x = 0.15 and 0.3)

S Krupička[1], Z Jirák[1,4], J Hejtmánek[1], M Maryško[1], P Novák[1], M M Savosta[2] and R Sonntag[3]

[1] Institute of Physics AS CR, Cukrovarnická 10, 162 53 Prague 6, Czech Republic
[2] Donetsk Institute of Physics & Technics, Academy of Sciences of Ukraine, Rozy Luxembourg 72, 340 114 Donetsk, Ukraine
[3] Hahn-Meitner-Institut, Glienicker Strasse 100, 14109 Berlin, Germany

E-mail: jirak@fzu.cz

Received 2 February 2001, in final form 4 May 2001
Published 19 July 2001
Online at stacks.iop.org/JPhysCM/13/6813

Abstract

An earlier study of the structural and magnetic transitions in $Pr_{0.5}Ca_{0.5-x}Sr_xMnO_3$ perovskites has been completed by a combination of the investigation of the NMR and transport properties together with a consistent application of a two-phase approach in the evaluation of the neutron diffraction data. The compositions with $x = 0.15$ and $x = 0.3$ were chosen as typical representatives for two different kinds of behaviour in the course of these transitions. For both compositions the existence of the first-order structural transition between the high-temperature pseudocubic and low-temperature charge-ordered tetragonally contracted low-temperature phases was found with critical temperatures $T_{co} = 210$ K and 200 K for $x = 0.15$ and $x = 0.3$, respectively. The coexistence of both phases below T_{co} was observed and their relative volumes were determined. Two different ^{55}Mn NMR FM signals were detected and one possessed a complex dynamics of nuclear spins. This signal was observed in both materials for $T < T_{co}$ and was ascribed to FM inclusions within the 1:1 Mn^{3+}/Mn^{4+} ordered phase with the CE-type antiferromagnetic ground state. The second signal, found for $x = 0.3$ only, was identified with ferromagnetism within the pseudocubic phase with $T_C = 215$ K and almost temperature-independent magnetization $\sim 2\mu_B$/Mn. Its appearance was found to be accompanied by a distinct phase separation of electronic origin, leading to stabilization of FM clusters below T_C. Due to the phase separation this second FM phase for $x = 0.3$ coexists with the PM phase, gradually increases its volume and, finally, vanishes with the onset of CE-type antiferromagnetism at $T_N^C = 170$ K ($T_N^W = 180$ K). A detailed study of the thermal and electronic transport in magnetic fields up to 5 T (9 T) has revealed the metallic character of small ferromagnetic clusters imbedded into an insulating matrix.

[4] Author to whom correspondence should be addressed.

0953-8984/01/316813+22$30.00

The influence of the magnetic field upon the overall electrical conductivity in various temperature ranges was investigated and the role of percolation discussed.

1. Introduction

Extensive studies of the colossal magnetoresistance (CMR) in mixed-valent manganites $Ln_{1-y}A_yMnO_3$ with a perovskite structure (Ln = La or RE, A = Ca, Sr, Ba) has revealed this effect to be usually connected with one of the following kinds of metal–insulator transitions: (i) between the ferromagnetic (FM) metallic and paramagnetic (PM) insulating states in the vicinity of the Curie temperature T_C [1–5]; and (ii) between the antiferromagnetic (AFM) charge-ordered (CO) insulating and FM metallic states close to the charge ordering (T_{co}) and/or AFM order (T_N) instabilities provided that $T_N \leqslant T_{co} < T_C$. The first kind of transition usually occurs in the vicinity of $y = 0.3$ compositions with orthorhombic symmetry for which the proximity of the border between the Jahn–Teller distorted O′-type phase with the normal O-type one is characteristic [5]. The second kind then relates to $y = 0.5$ compositions such as $RE_{0.5}Sr_{0.5}MnO_3$ [6–8].

The mentioned transitions and accompanying effects are found to be very complex, being the result of a delicate interplay of a large number of electronic (charge, spin, orbital) and lattice degrees of freedom. In particular, many recent papers dealing with CMR materials have reported strong evidence of the unusual effects of phase separation which seems to be an essential attribute of the metal–insulator transitions in the perovskite manganites. The intrinsic nature of these effects has been supported by theoretical considerations including numerical calculations (see, e.g., [9]). It appears that the actual separation (or segregation) can be of different kinds—on a nanometre scale, especially if the separated phases possess different charge densities [10–12]; or on a larger (micrometre) scale if the charge density remains constant [13–15]. The phase separation is not limited to a coexistence of the FM and PM or CO AFM phases only; namely, a simultaneous presence of both the metallic and polaronic regions in apparently bulk FM systems has been generally reported [16–19].

In any case, the course and the character of the phase separation depends strongly on many material parameters and external fields. The basic intrinsic parameter is probably the tolerance factor t which describes the mismatch of the (Ln,A)–O and Mn–O ionic bonds in the ideal cubic perovskite. The most usual way to study the influence of t is to combine two kinds of either trivalent Ln cations with different ionic radii, for example La^{3+} and Nd^{3+}, or to do the same with divalent A cations, for example Sr^{2+} and Ca^{2+}. The present $y = 0.5$ system $Pr_{0.5}Ca_{0.5-x}Sr_xMnO_3$ is an example of the latter possibility. The end members of this system, $Pr_{0.5}Ca_{0.5}MnO_3$ and $Pr_{0.5}Sr_{0.5}MnO_3$, have been frequently studied [20–22] and may be taken as model compounds. They exhibit very different characteristics including different crystallographic space groups and types of the low-temperature AFM state. This involved a detailed investigation concerning the way in which the properties were transformed when going from one end ($x = 0$) to another ($x = 0.5$) [23, 24].

Our former studies of $Pr_{0.5}Ca_{0.5-x}Sr_xMnO_3$ [25] have confirmed much complexity in both the crystallographic properties and magnetic behaviour across this series, $0 \leqslant x \leqslant 0.5$. Even within the subregion of $Pbnm$ symmetry ($0 \leqslant x \leqslant 3.5$) one encounters important differences: while the $x = 0$ material, when cooled, goes over from the charge-disordered PM state through a sequence of incommensurately modulated ordered structures ($T_{co} = 250$ K) into a CE-type antiferromagnetism ($T_N = 170$ K) [20], the compositions close to $x = 0.3$ are

first FM below $T_C = 215$ K, becoming CE-type CO antiferromagnets by a first-order transition below ∼170 K. In the intermediate compositions ($0.1 \leqslant x \leqslant 0.25$), the CO CE-type AFM state is preceded by a rather broad two-phase temperature region where the minority FM phase coexists with the majority CO PM ones [25]. The composition $x = 0.15$ may be taken as typical of this behaviour.

As to the occurrence of bulk ferromagnetism for $x = 0.3$, a recent NMR study [26] has shown that the PM to FM transition also possesses a first-order character with coexisting FM and PM phases. Moreover, two distinct signals were found in the NMR spectra in the course of increasing temperature, which points to the complex character of the FM phase and its spacial diversity. These novel findings made us reinvestigate the former neutron diffraction data in order to find a compatible structural model. Some complementary NMR experiments were carried out in parallel. Taking into account the role of ferromagnetism in the electron transport properties of the mixed-valence manganites, it also appeared important to investigate more thoroughly the relation between the magnetic state and the electrical resistivity and other transport properties, including the magnetoresistivity effects in the vicinity of the FM ↔ AFM transitions. The present paper summarizes the results of all the complementary studies we carried out on the compositions $x = 0.15$ and $x = 0.3$ which are typical for two different subregions in the $Pr_{0.5}Ca_{0.5-x}Sr_xMnO_3$ magnetic phase diagram. Among others, it newly interprets the FM state on the basis of FM phase segregation.

2. Experimental

The preparation and general characterization of ceramic samples $Pr_{0.5}Ca_{0.5-x}Sr_xMnO_3$ ($x = 0.15$ and 0.3) used in the present study has been described in [25]. A complete determination of the crystal and magnetic structures and their temperature evolution has been performed on the diffractometer E3 in BENSC, Hahn-Meitner-Institut, Berlin. The diffraction patterns were taken using the wavelength $\lambda = 1.228$ Å in a temperature range 2–300 K both for the heating and cooling runs. The data were processed with the help of a profile analysing program FULLPROF. The structural refinement included two perovskite phases of the *Pbnm* symmetry (the high-temperature pseudocubic phase and the CO phase with characteristic pseudotetragonal lattice contraction) and the respective magnetic orderings (FM and CE-type AFM).

Some complementary measurements of the dc magnetic moments were performed using a SQUID magnetometer (Quantum Design, MPMS-5S) and the RESET option ($H_{dc} < 2$ Oe) in the case of zero-field cooled (ZFC) experiments. In some cases the magnetic moment and the electrical resistivity were measured simultaneously.

The magnetothermal (thermoelectric power and thermal conductivity) and magnetoelectric transport measurements were carried out using the PPMS Quantum Design System within the temperature range 5–320 K up to 9 T. Standard four-probe steady-state methods were used. In the thermal measurements, the measuring and power contacts were separated, which eliminated the thermal resistances between the sink and the heater, respectively. The rectangular shaped sample was affixed on the cell mounted on the PPMS puck and the miniature resistor heater, charged using a pair of 72 μm chromel wires, was attached by GE varnish on the sample extremity. The temperature gradient and voltage drop was monitored using two separated differential chromel–constantan thermocouples (72 μm in diameter) which were affixed to the sample using indium solder. With respect to the sensitivity of the used thermocouples, a temperature difference of $\Delta(T) = 0.5 + 0.005T$ (K) was applied across the sample. The influence of the magnetic field on the measured temperature gradient and the thermopower of chromel was calibrated using the reference non-magnetic (high temperatures)

and superconducting (low temperatures) samples. The perceptible impact of the magnetic field on the measured thermal gradient and thermovoltage for temperatures below 20 K was observed and corresponding corrections were made.

The ^{55}Mn NMR spectra were registered by a two-pulse spin-echo method at temperatures between 77 and 220 K using a non-coherent spectrometer with frequency sweep and boxcar detector signal averaging. The value of the radio frequency (rf) field required for the maximum echo signal of ^{55}Mn was found to be characteristic of resonance coming from FM domains. In order to take into account the effect of the spin–spin nuclear relaxation on the NMR spectra, at each temperature the data were collected for several time intervals τ between the exciting and refocusing rf pulses. The experimental technique as well as the method of data evaluation have been described elsewhere [26, 27].

3. Results

3.1. Neutron diffraction

The neutron diffraction experiments have shown that the samples $Pr_{0.5}Ca_{0.5-x}Sr_xMnO_3$ ($x = 0.15$ and 0.3) exhibit the tilt pattern of the orthorhombic symmetry $Pbnm$ ($GdFeO_3$ perovskite-type structure) and the same CE-type AFM ground state at low temperatures. In the $x = 0.3$ sample, the antiferromagnetism is preceded by a temperature interval of essentially bulk ferromagnetism ($T_C = 215$ K).

In the preliminary analysis of the neutron diffraction of $x = 0.15$ and 0.3 we assumed a quasi-homogeneous change of the lattice parameters during the phase transitions. Most of the results obtained in this way were published in [25]. Both the FM–AFM and the disordered to CO state transitions then appeared as coupled for $x = 0.3$, with a large hysteresis manifested in the temperature dependence of the lattice parameters. While the onset of the transition was abrupt in the $x = 0.3$ case, it was rather smooth for $x = 0.15$. In the latter case the transitions to AFM and CO states were decoupled, however, as the charge ordering had already originated in the PM phase ($T_{co} = 210$ K) and the characteristic lattice deformation developed gradually towards lower temperatures.

This basically single-phase approach obviously represents a fairly good approximation for both the high-temperature and low-temperature regions. But when we apply it for temperatures in the vicinity of the CO and/or magnetic phase transitions we may meet with some inconsistencies, especially when distinct crystallographic phases are present. Therefore, taking into account recent evidence of the phase separation in the CO systems [5, 9, 13, 18, 28], we re-evaluated the diffraction patterns using a two-phase model in which the CO tetragonally contracted regions coexist with the high-temperature pseudocubic phase. Even if the phase coexistence was not obvious on the diffraction patterns because of limited resolution, the profile analysis by the FULLPROF program gave at least for the $x = 0.3$ sample reliable results in favour of the two-phase model. Moreover, some spurious effects which occurred in the previous single-phase refinement, e.g. the sharp minimum of the unit cell volume at T_{co} (see [3]), have now been removed. The results for both $x = 0.15$ and 0.3 are displayed in figure 1 where the temperature dependences of the lattice parameters (upper panels) and volume fractions of the pseudocubic and CO deformed phases (lower panels) are given. The coexistence of the charge-disordered pseudocubic phase with the CO tetragonally contracted phase is clearly visible in both the $x = 0.15$ and 0.3 compositions. The volume fractions of both phases exhibit a considerable thermal hysteresis. At low temperatures the charge ordering is not complete, which points to the existence of about 5% of the pseudocubic phase for $x = 0.3$ and, similarly, of about 10% for $x = 0.15$. While the result for $x = 0.3$ is fully consistent with

the value of the residual low-temperature FM moment determined by magnetic measurements [25] and by NMR [26], the mentioned pseudocubic fraction of 10% for $x = 0.15$ exceeds the volume of the parasitic FM regions deduced from magnetic measurements (about 4%).

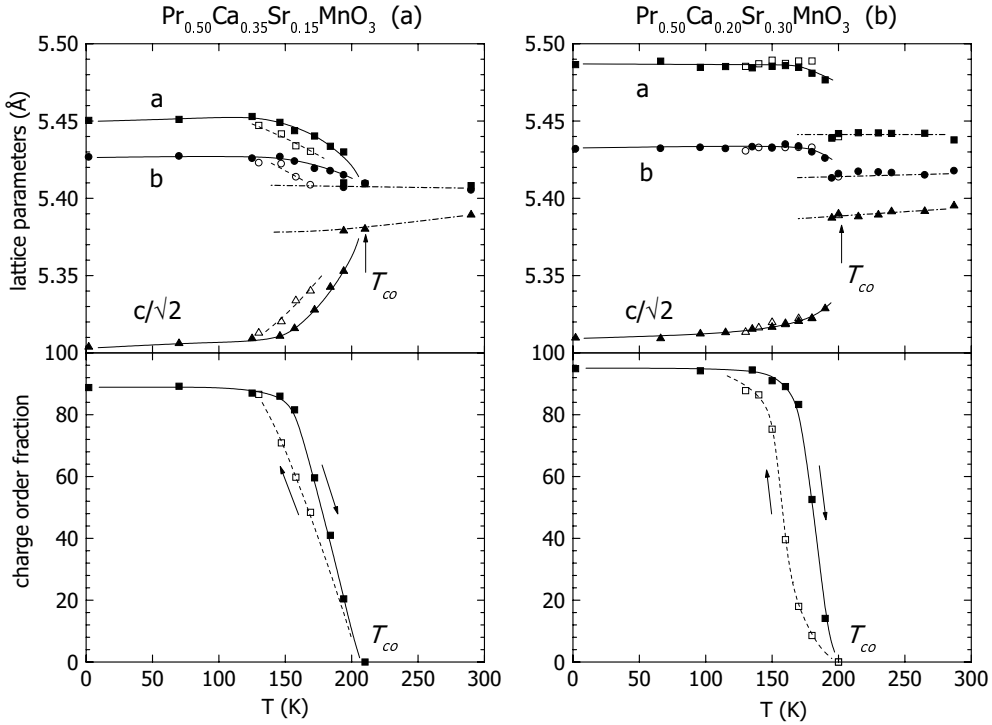

Figure 1. Basic crystallographic data obtained by the two-phase analysis of the neutron diffraction patterns for (a) $x = 0.15$ and (b) $x = 0.3$. The upper panels show the temperature dependences of the lattice parameter of both phases; the lower panels show the corresponding volume fractions.

The critical temperatures (T_{co}) at which the tetragonally deformed phase first appears are 210 K and 200 K for $x = 0.15$ and 0.3, respectively. The first value is about 10 K lower than T_{co} determined previously for $x = 0.15$ by the magnetic susceptibility measurements while the second exactly corresponds to the extrapolated value of the $T_{co}(x)$ for $x \to 0.3$ [25].

The temperature dependences of the lattice parameters in the upper panels of figure 1 are different for $x = 0.15$ and 0.3. In the latter case, they exhibit an abrupt change at T_{co} typical of a first-order transition. Moreover, the thermal hysteresis of the lattice parameters observed for the single-phase model [25] has disappeared being substituted by the hysteresis in the volume fractions of the pseudocubic and the CO (tetragonally deformed) phases. For $x = 0.15$, however, the temperature changes of lattice parameters remain gradual and still exhibit hysteresis. This is probably a consequence of the gradual course of the charge ordering, possibly through a sequence of incommensurate configurations analogous to the previously reported case of $x = 0$ [20]. The results further show that the low-temperature CO phase in both samples exhibits a unit cell volume which is lower by about 0.25% compared with the pseudocubic disordered phase. The variation of the respective volumes with temperature cannot be determined with accuracy.

In contrast to the crystallographic properties the evaluation of magnetic neutron diffraction data using the present two-phase model is neither simple nor straightforward. The simplest

model would attribute the antiferromagnetism to the CO regions, leaving the rest (i.e. the undistorted pseudocubic phase) to the bulk ferromagnetism or paramagnetism according to whether $T < T_C$ or $T > T_C$. But this cannot be fully satisfactory because of a phase separation found below T_C in the $x = 0.3$ case [26] and, also, the slightly different succession of the corresponding critical temperatures ($T_N < T_{co} < T_C$ for $x = 0.3$; $T_N < T_C < T_{co}$ for $x = 0.15$). On the other hand, such a simple model may yield quite reliable results for the AFM regions ($T \leqslant T_N$) concerning the values of the ordered magnetic moments. The temperature dependences of the moments are shown in figure 2 (for the CE-type state only the average over Mn^{3+} and Mn^{4+} sites are displayed). In both compositions a thermal hysteresis is clearly visible pointing to different Néel temperatures for cooling and warming runs: $T_N^C = 155$ K, $T_N^W = 170$ K for $x = 0.15$ and $T_N^C = 170$ K, $T_N^W = 180$ K for $x = 0.3$. As the AFM moments in figure 2 are renormalized to the volume of the CO phase, their hysteresis cannot be ascribed to the hysteresis in the volume of this phase displayed in figure 1 and should be seen as connected with the magnetic state of the AFM phase and its defects. A more thorough analysis of the $T = 2$ K data yields for AFM ordered magnetic moments of Mn^{3+} and Mn^{4+} sublattices in $x = 0.15$ the values of 2.51 μ_B and 2.77 μ_B, respectively; the values for $x = 0.3$ are 2.98 μ_B and 2.85 μ_B. While the AFM moments are aligned along the a-axis of the $Pbnm$ cell for $x = 0.3$, they are inclined to about 30° from the a-axis towards the b-axis for $x = 0.15$. The inclination, low value of the Mn^{3+} moments and the broadening of some magnetic lines point to some residual incommensurity of the CO state in the $x = 0.15$ sample (see, e.g., [20]).

The only FM contribution detected in our neutron diffraction experiments has been the FM phase in $x = 0.3$ appearing below $T_C = 215$ K and quickly disappearing below T_N. In spite of this, the coexistence of FM and AFM phases in a narrow temperature region below T_N is clearly seen in figure 2(b). The residual ferromagnetism surviving to low temperatures and detected in both magnetic and NMR measurements [25, 26] has not been found, however, due to the limited sensitivity of the neutron diffraction and/or small extension of FM domains. The same can be said about the FM phase for $x = 0.15$, which according to [25] coexists with the PM phase in a narrow temperature region below $T_C \approx 200$ K.

At first sight it would seem quite natural to identify the FM phase for $x = 0.3$ with the pseudocubic phase. The temperature dependence of the actual FM moment would then be that in figure 2(b) which has been renormalized to the real volume of the pseudocubic phase displayed in figure 1(b). But in reality the situation is more complicated: according to NMR data [26] the development of the ferromagnetism below T_C is gradual, being accompanied by a separation of the FM and PM phases. Therefore, the ferromagnetism fills only partly the whole volume which is taken up by the pseudocubic phase.

3.2. Nuclear magnetic resonance

For $x = 0.3$, most of the NMR data and their analysis are described in [26]. The results relevant to the present study can be summarized as follows: two different FM NMR lines denoted as A and B were observed at low and high temperatures, respectively, being coexisting in a certain temperature interval. Moreover, it was found that the width of line A depends on the experimental conditions; with increasing the time interval τ, the linewidth becomes first smaller, but remains constant after surpassing a certain value of τ. To take into account this behaviour, line A was replaced by two unresolved lines A_1 and A_2 with different spin–spin relaxation times T_2. In figure 3(a) is the lineshape of NMR spectra obtained at different τ ($T = 155$ K, cooling run) and the decomposition of the spectrum at $\tau = 3$ μs on three lines are displayed. The temperature dependence of the resonance frequency of lines A_1, A_2 and B are shown in figure 4(a). While F_{A_1} and F_{A_2} exhibit a marked dependence on temperature,

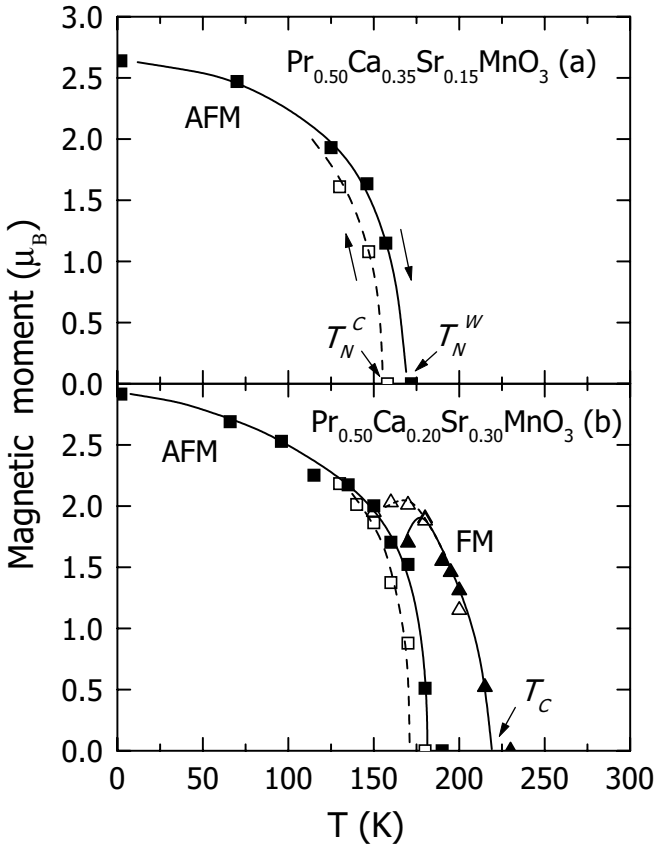

Figure 2. Temperature dependences of magnetic moments for (a) $x = 0.15$ and (b) $x = 0.3$ as determined from neutron diffraction for the two-phase model. In (a) only the AFM moment is detected, in (b) both AFM and FM moments are shown. In the evaluation of (b) it was assumed that below T_C all the pseudocubic phase is ferromagnetically ordered.

including hysteresis, F_B differs in this point being almost temperature independent. In figure 4(b) the temperature dependence of the relative volume of the FM regions corresponding to the lines A_1+A_2 and B are displayed. The volumes were deduced from the integral intensities of the lines after correcting them for both the change of enhancement factors and the $1/T$ dependence of the spin-echo intensity [26].

The line B appears below $T_C = 215$ K. The corresponding volume develops dramatically with decreasing temperature reaching maximum at about 170 K, i.e. in the vicinity of T_N^C. Then it falls rapidly and disappears closely below 150 K. On warming there exists a thermal hysteresis of about 15 K on the low-temperature side while for $T > 180$ K the behaviour is non-hysteretic. Let us note that the corresponding resonance frequency F_B exhibits no hysteresis at all. According to these characteristics the signal B has been ascribed to the majority FM phase which was previously reported below T_C in both the magnetic and neutron diffraction experiments [25]. A very striking result of the present analysis is the finding that it is the change in the volume of the FM phase B which is almost fully responsible for the temperature dependence of the net magnetization, the local magnetic moments being nearly constant within the whole temperature interval 150 K $< T < T_C$.

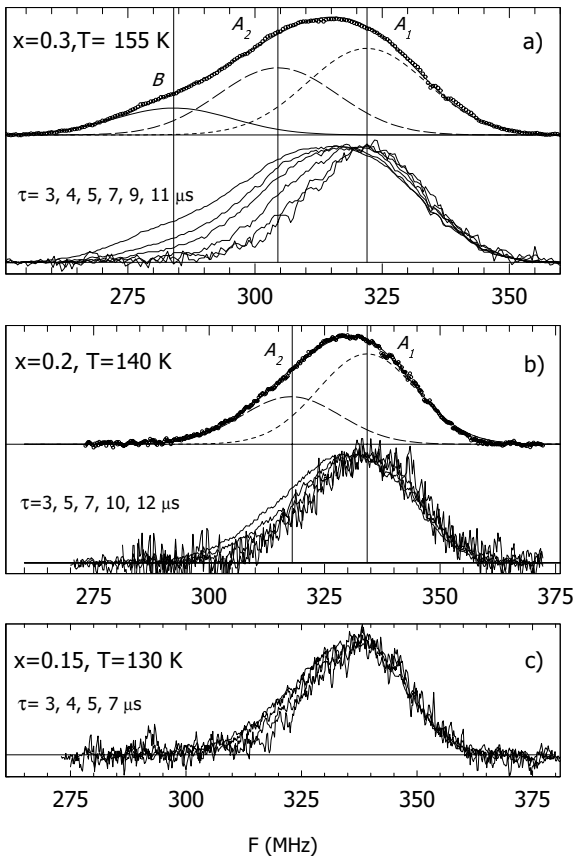

Figure 3. For $Pr_{0.5}Ca_{0.5-x}Sr_xMnO_3$ the selected NMR spectra of ^{55}Mn taken for different values of the time interval τ between the exciting and refocusing rf pulses at cooling. The amplitudes are normalized to show the evolution of the lineshape. The width of the spectra first decreases when increasing τ, then generally remains constant giving rise to the A_1 line. Based on this behaviour, spectra are decomposed on three ($x = 0.3$, $\tau = 3$ μs) and two ($x = 0.2$, $\tau = 3$ μs) lines, respectively.

The minority FM signal A_1 starts at about 200 K. This temperature coincides with the appearance of the deformed CO phase, i.e. T_{co} (see figure 1(b)). The signal A_2 may be distinguished in the NMR spectra starting from ≈170 K. While B disappears at a definite temperature, both A_1 and A_2 persist down to low temperatures. The A_1/A_2 phase ratio seems to vary even in that temperature range. The overall A phase volume exhibits a substantial thermal hysteresis (figure 4(b)) which is evidently conditioned by the presence of the coexisting AFM phase.

In contrast to $x = 0.3$, no bulk (or at least prevailing) FM phase has been observed in $x = 0.15$. Indeed, the NMR spectra include no signal that could be compared with line B. On the other hand, line A was detected for the temperature range below ≈180 K where the minority FM regions coexist with the CO phase which is PM above T_N (155 K on cooling, 170 K on warming) and AFM below. The width of line A depends on time interval τ in a similar manner as for the $x = 0.3$ sample (see figure 3(c)). In this case, however, unambiguous A_1, A_2 decomposition would be very difficult as, due to the small intensity of the signal, we did not succeed in reaching the lineshape corresponding to the A_1 signal when increasing

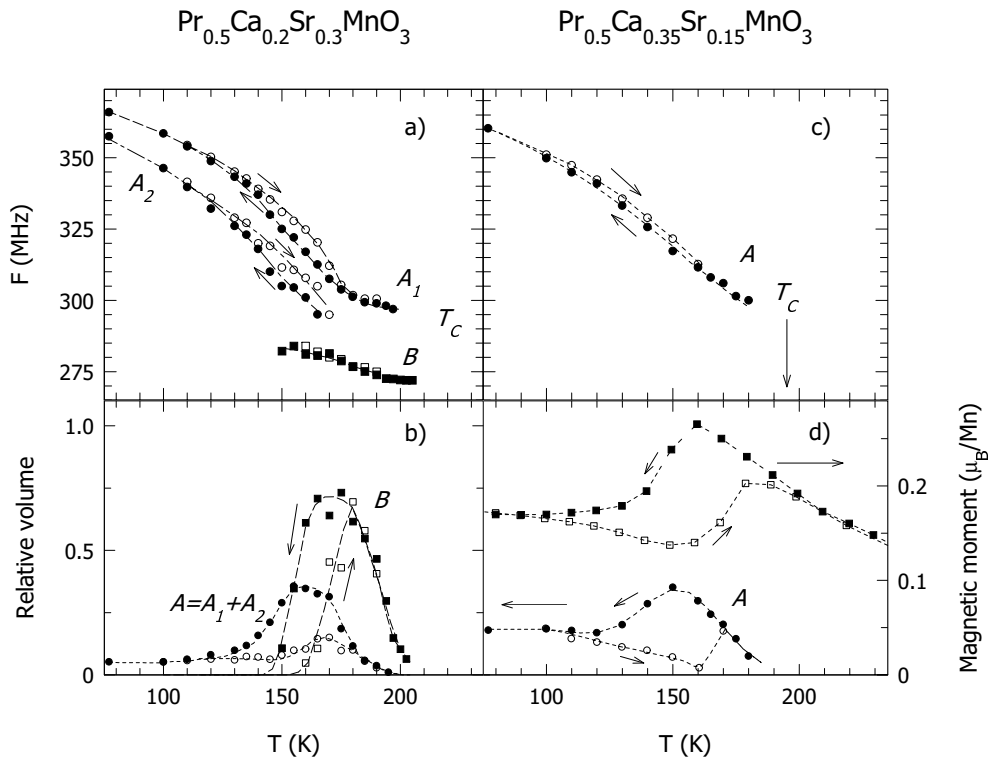

Figure 4. Temperature dependences of ^{55}Mn NMR data for $x = 0.3$ (a,b) and $x = 0.15$ (c,d) both for cooling (full symbols) and warming (open symbols). The curves serve as guides for the eyes only. (a) Resonance frequency for three FM signals A_1, A_2, B obtained from a decomposition of the ^{55}Mn NMR spectra. (b) Relative volumes of two FM phases A and B corresponding to areas under curves $A_1 + A_2$ and B. (c) Centre of gravity of the A line. The value $T_C = 195 \pm 5$ K for $x = 0.15$ was deduced from the magnetic measurements [25]. (d) Relative volume of the FM A phase obtained from the integral intensity of NMR spectra. The temperature dependence of the A-phase volume as seen by NMR is compared with magnetization at $B = 0.75$ T.

τ. To demonstrate that the problem is technical rather than physical, we show in figure 3(b) the separation based on a different relaxation behaviour of A_1 and A_2 for the composition $x = 0.2$ which according to [25] exhibits a magnetic behaviour close to $x = 0.15$. For the above reasons, the temperature dependence of the resonance frequency in the $x = 0.15$ sample displayed in figure 4(c) relates to the centre of gravity of the unresolved signal A. Also, the temperature dependence of the relative volume of the FM phase (figure 4(d)) was deduced from the integral intensity of the NMR spectra, extrapolated to $\tau \to 0$. Note that above $\sim$150 K the line starts to narrow, which indicates that part of the nuclei (line A_2) relaxes too fast to be detected even at the shortest τ. Accordingly, the NMR leads to a systematic underestimation of the FM phase volume for $T > 150$ K.

Looking back on figures 3 and 4 and comparing the main characteristic features of A_1 and A_2 for $x = 0.3$ with those for $x = 0.15$ we see that the origin of the A signals is very probably analogous for both $x = 0.15$ and 0.3.

3.3. Electronic and thermal transport; magnetoresistance

The behaviour of the thermopower $\alpha(T)$ and the electrical resistivity $\rho(T)$ during temperature cycles between 10 K and 300 K and back are displayed in the upper and middle panels of figure 5, respectively, both for zero and 5 T applied fields. Each cycle lasted about 30–35 h, which seemed to be sufficient for a quasistatic measurement, at least for $T \geqslant 100$ K (a typical relaxation time at $T \approx 100$ K was about 20 min). In the absence of magnetic field the resistivity values below ≈60 K were too high to obtain reliable results and that is why the corresponding points were omitted in the figure. On the other hand, the trend of $\alpha(T)$ to reach values close to zero at $T \leqslant 50$ K obviously reflects a physical reality as will be discussed later. All the measured dependences are conspicuous for their large thermal hysteresis, the $\rho(T)$ for $x = 0.15$ being an exception provided that it is measured in zero magnetic field. In order to persue the possible relation between the transport properties and the magnetic state, the magnetization values at 0.75 T and 5 T, measured in similar temperature cycles, are shown in the lower panels of figure 5. For $x = 0.3$, the thermoelectric power $\alpha(T)$ evidently tends to become closer to zero when the temperature is lowered from T_C to T_N^C, the minimum negative value of about -15 μV K^{-1} is reached at ≈160 K on cooling, i.e. close to T_N^C. A similar extreme exists for warming in the vicinity of T_N^W. This indicates the quasimetallic character of the type-B FM domains whose overall volume increases from T_C to T_N according to NMR results. A similar, but much weaker effect of this kind can be observed for $x = 0.15$ where only the minority A-type ferromagnetism is detected by NMR. In both cases the flat, almost linear part of the $\alpha(T)$ curve between T_C and T_N is followed by an abrupt decrease of α towards lower T, which can be compared with the rapid decrease of the FM moment below T_N. On the other hand, the magnetic field of 5 T substantially reduces this decrease in $\alpha(T)$ without any effect of comparable magnitude upon magnetization $M(T)$. Let us note that for $B = 9$ T the thermoelectric power $\alpha(T)$ continues smoothly its metallic-like course approaching zero for $T \to 0$.

In zero magnetic field, the electrical resistivity of both compositions exhibits a thermally activated temperature course ($\mathrm{d}\rho/\mathrm{d}T < 0$) along the whole measuring cycle and, for all temperatures, the $\rho(T)$ of $x = 0.15$ is larger than the $\rho(T)$ of $x = 0.3$. As may be further inferred from the figure, the $\rho(T)$ curves reflect changes associated with the destruction or reappearance of the FM order on cooling or warming, respectively. But even more the relation between the resistivity and the magnetic state is evidenced by a pronounced effect of a strong magnetic field (5 T). In particular, $\rho(T)$ becomes practically temperature independent for low temperatures and metallic-like for both compositions. Note that these low-temperature values of resistivity are surprisingly smaller for $x = 0.15$ compared with $x = 0.3$.

In order to have a look from the other side, we also measured the thermal conductivity λ of both materials using the same temperature cycle as before (figure 6). Although λ does not characterize the electron transport but the thermal one, it may include a considerable electron contribution, provided the electrical conductivity is metallic-like. We see in the figure that the $\lambda(T)$ curve for $x = 0.15$ in zero field is without any clear-cut thermal hysteresis while the curve for $x = 0.3$ possesses a hysteretic hump which correlates well with the existence of the FM phase B. Hence, we can naturally ascribe its origin to the electron contribution λ_e to λ. In a strong magnetic field, a similar anomaly appears even for $x = 0.15$ indicating a probable conversion of the A-type ferromagnetism into the B-type or the bulk one due to the magnetic field effect (cf the $M(T)$ curves in the lower panels of figure 5). The thermal hysteresis of the λ_e contribution is then to be ascribed to the hysteresis in the relative volume of the FM phase.

A substantial reduction of the electrical resistivity in the magnetic field shown in figure 5 points to the existence of a remarkable magnetoresistance. In figures 7 and 8 the resistivities as

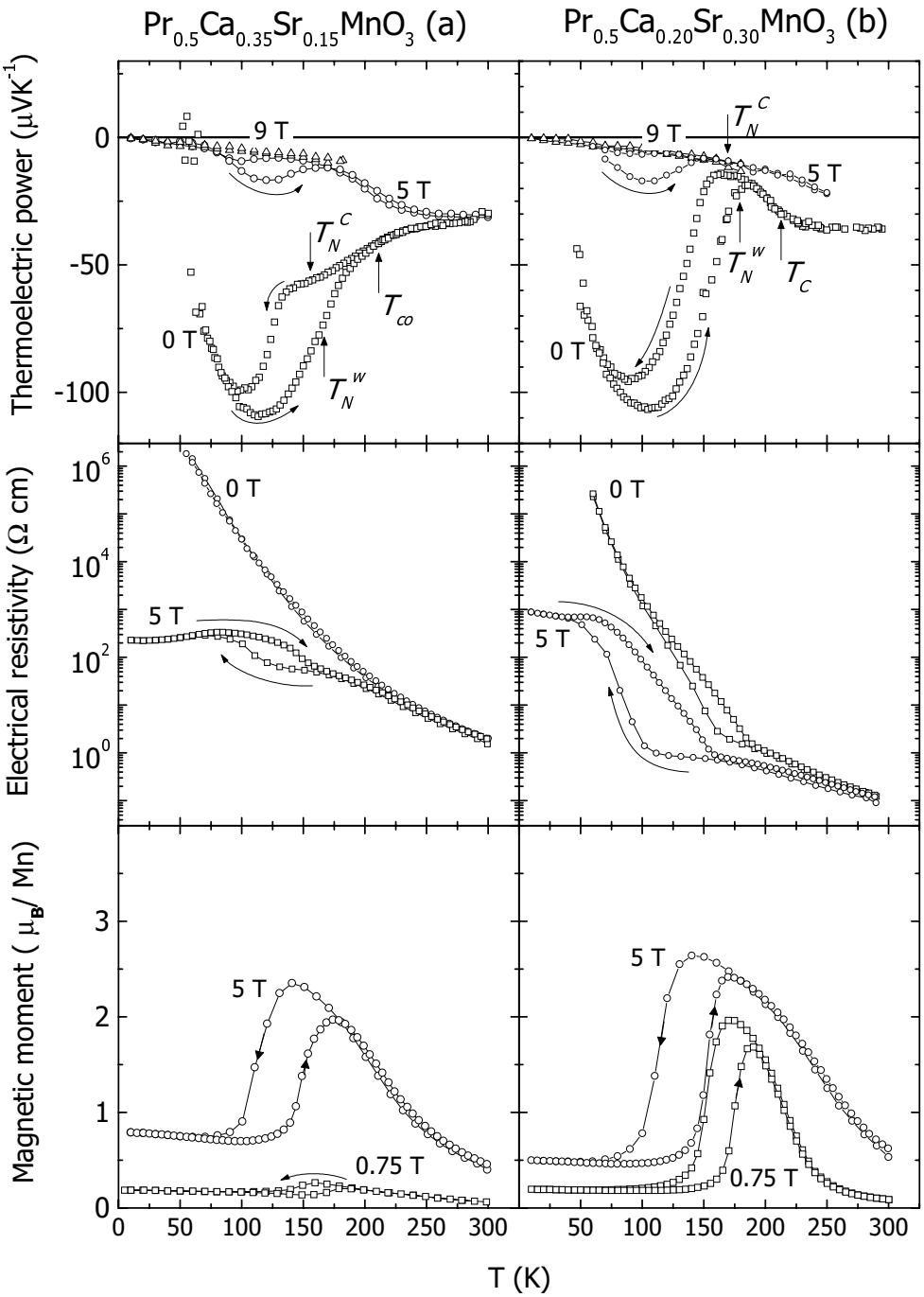

Figure 5. The temperature dependences in 0 T and 5 T magnetic fields of the thermopower α and electrical resistivity ρ (upper and middle panels, respectively) compared with the temperature dependences of magnetization measured at 0.75 T and 5 T (lower panels): (a) $x = 0.15$; (b) $x = 0.3$. The results at 9 T are also shown for α.

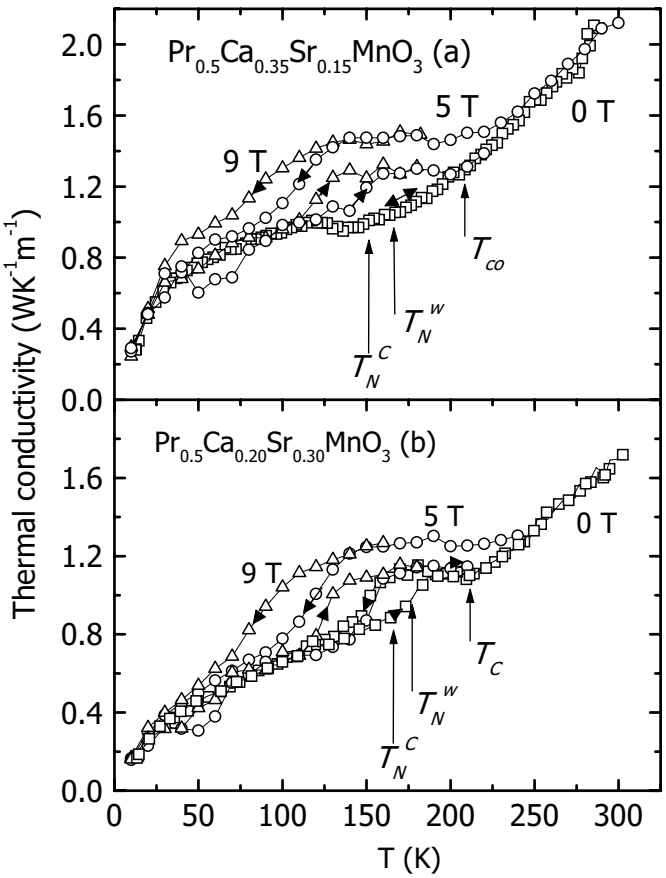

Figure 6. Thermal conductivity λ against temperature for (a) $x = 0.15$ and (b) $x = 0.3$ in 0 T, 5 T and 9 T magnetic fields.

a function of the magnetic field, taken at several representative temperatures, are shown for both the compositions $x = 0.15$ and 0.3. They are confronted with magnetization loops measured simultaneously. Beside a low-temperature irreversible behaviour of both the resistivity and magnetization after cooling in the zero field (ZFC), two effects can be distinguished: the magnetoresistance in low fields which manifests itself by a non-zero slope $\mathrm{d}\rho/\mathrm{d}H$ in fields $0\ \mathrm{T} \leqslant B \leqslant 1\ \mathrm{T}$, and the magnetoresistance in higher fields, $B > 1$ T. The first effect is rather small and it is primarily connected with orientation of the magnetization into the magnetic field direction. The second is clearly visible in the composition with $x = 0.15$ at higher temperatures where $\mathrm{d}\rho/\mathrm{d}H \sim 0$ for $B = 0$ and an appreciable magnetoresistance starts at $B \sim 1$ T. The form of the corresponding magnetization curves and thermal hysteresis in both the magnetization and resistivity point to a metamagnetic phase transition. The irreversibility at low temperatures already mentioned is due to the difference between the ZFC and FC low-temperature states [25]. Note that the 'true' magnetoresistance measured on field cycles at constant T as shown in figures 7 and 8 is for low temperatures much smaller than the difference $\rho(B = 0) - \rho(B)$ taken from measurements on temperature cycles with constant B (figure 5). This is also evident from figure 9 where a temperature dependence of the magnetoresistance is compiled from figures 7 and 8 as the ratio $\rho(B = 0)/\rho(B = 5\ \mathrm{T})$.

For both compositions a characteristic peak in the magnetoresistance exists in the vicinity of the FM–AFM transition [6, 23]. It obviously originates from a shift of the corresponding critical temperature in the presence of a magnetic field. For $x = 0.15$, however, this may be combined with the metamagnetic transitions already discussed in connection with figure 7 and similar effects associated with weakly coupled spins at low temperatures [25].

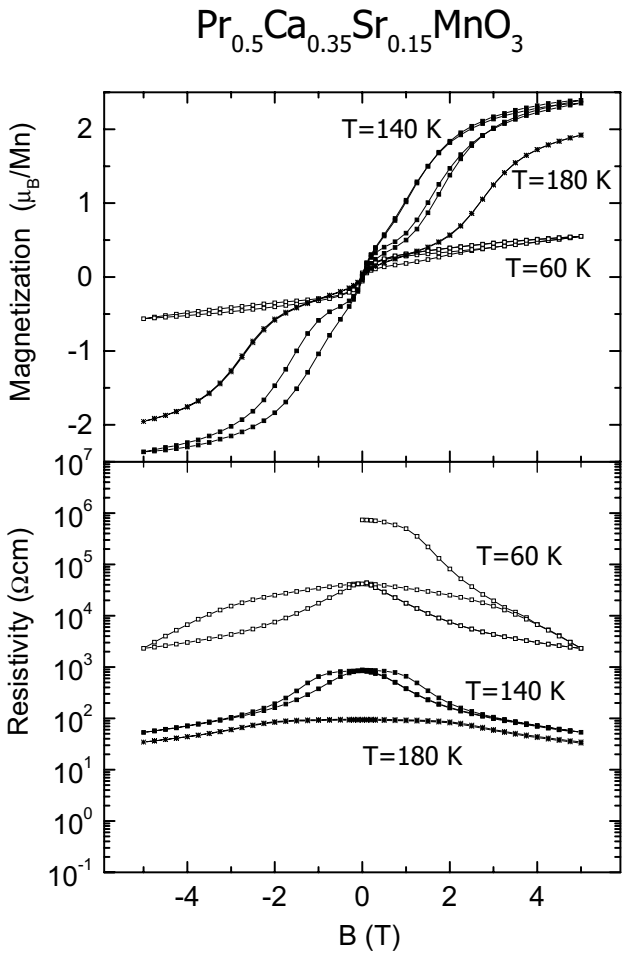

Figure 7. Typical resistivity and magnetization isothermal loops for $x = 0.15$ in magnetic field up to 5 T.

In order to complete the picture, the thermoelectric power and thermal conductivity as functions of applied magnetic field measured at several constant temperatures are shown in figure 10. They represent a counterpart to the magnetoresistance and magnetization loops in figures 7 and 8 and are to be compared with them. While at higher temperatures (typically $T \approx 180$ K), the magnetic field of 5 T is sufficient to complete the FM ordering in both compositions and to saturate both α and λ to their quasimetallic values, no such saturation effect exists for λ at $T \geqslant 100$ K, even if the magnetic field is increased up to 9 T. This points to the absence of magnetic saturation in this temperature range and, therefore, to a mere percolative character of the electronic transport between metallic-like FM clusters embedded in an insulating AFM matrix. Such a conclusion is also supported by the metallic-like character

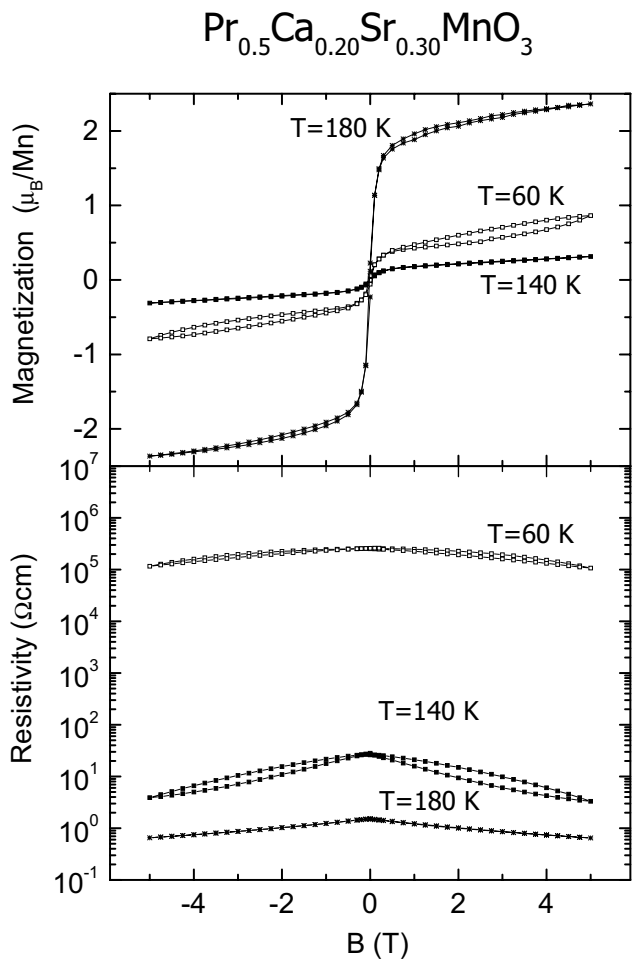

Figure 8. Typical resistivity and magnetization isothermal loops for $x = 0.3$ in magnetic fields up to 5 T.

of both the electrical conductivity and thermopower in the magnetic field of 5 T at temperatures below 100 K for both compositions (figure 5).

4. Discussion

The application of a two-phase model in evaluating the neutron diffraction patterns has confirmed the existence of a first-order structural transition for both $x = 0.15$ and 0.3 between the high-temperature pseudocubic disordered phase and the low-temperature charge (and orbitally) ordered, tetragonally deformed phase. This brings about two things: first, the critical temperature T_{co} for charge-order instability can be meaningfully defined even for the apparently 'coupled' transitions in the $x = 0.3$ case. Second, both of crystallographically different phases coexist in a certain temperature interval below T_{co} and, moreover, some small residual fraction of the high-temperature quasicubic phase survives to the lowest temperatures. This all represents the basic structural frame for the electronic and magnetic changes described in preceding paragraphs.

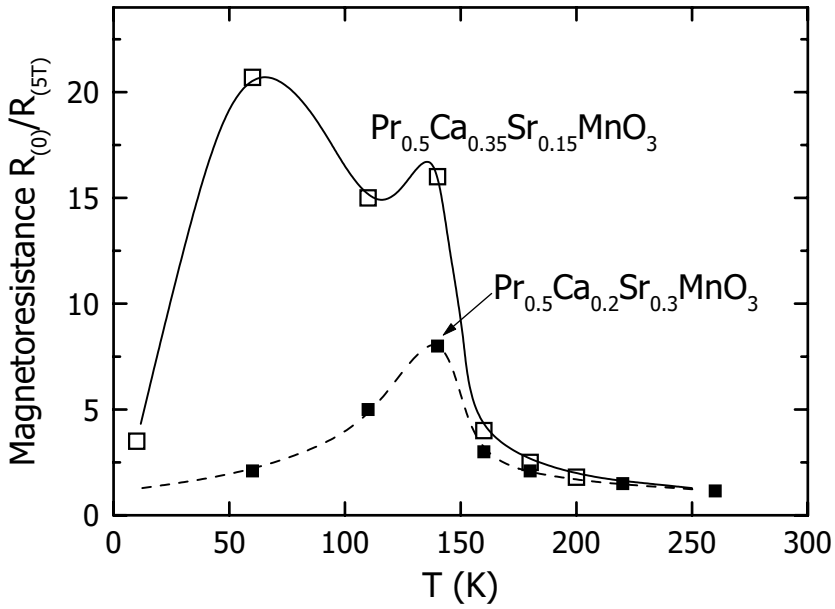

Figure 9. The magnetoresistance ratio $\rho(B = 0)/\rho(B = 5\ \mathrm{T})$ determined from the isothermal loops as in figures 7 and 8. Two effects can be distinguished—the peak at about 140 K related to the shift of charge-ordering temperature and, for $x = 0.15$, the low-temperature maximum due to polarization of the magnetically disordered regions and their electric percolation.

By far the most interesting of these effects are connected with the appearance, evolution and disappearance of the ferromagnetism. According to NMR results, two different kinds of ferromagnetism denoted by A and B were observed. For $x = 0.3$, both appear, partially simultaneously, while only A was found for $x = 0.15$.

The B phase appears at 215 K and its volume fraction grows gradually when the temperature is lowered. This means that even though only one crystallographic phase (the pseudocubic one) is detected for 200 K $< T <$ 215 K, two magnetic phases (the FM B and the PM one) coexist in this temperature interval. By combining the NMR results with direct spontaneous magnetization measurements we are able to make a quantitative estimate of the volume fraction of the overall FM phase ($B + A$) under the following assumptions: (i) the ratio of the local FM moments $\mu(B)$:$\mu(A_1)$:$\mu(A_2)$ is the same as that for the corresponding NMR frequencies F_B:F_{A_1}:F_{A_2} (see figure 4(a)); and (ii) the FM order is established over the whole pseudocubic phase at $T_N^C = 170$ K on cooling. The resulting local spontaneous FM moment then turns out to be around $2\mu_B$ and varies weakly with temperature for $T > 150$ K (see the inset of figure 11). The determined volume fraction of the FM phase as a function of temperature is shown in figure 11 where it is compared with the neutron diffraction data for the relative volume of the pseudocubic phase. While for cooling both the independently determined data are fully compatible, the calculated values for warming are systematically higher compared with the volume of the pseudocubic phase determined by the neutron diffraction. This discrepancy may be explained as follows: as the number of FM domains is strongly reduced at low temperatures, new domains nucleate on warming. These nuclei of the FM phase (or part of them) can be eventually smaller than the critical dimensions for the crystallographically coherent domains that can be detected by neutron diffraction, i.e. less than 1000 Å. Hence, although their magnetic moments contribute to the overall magnetization determined by

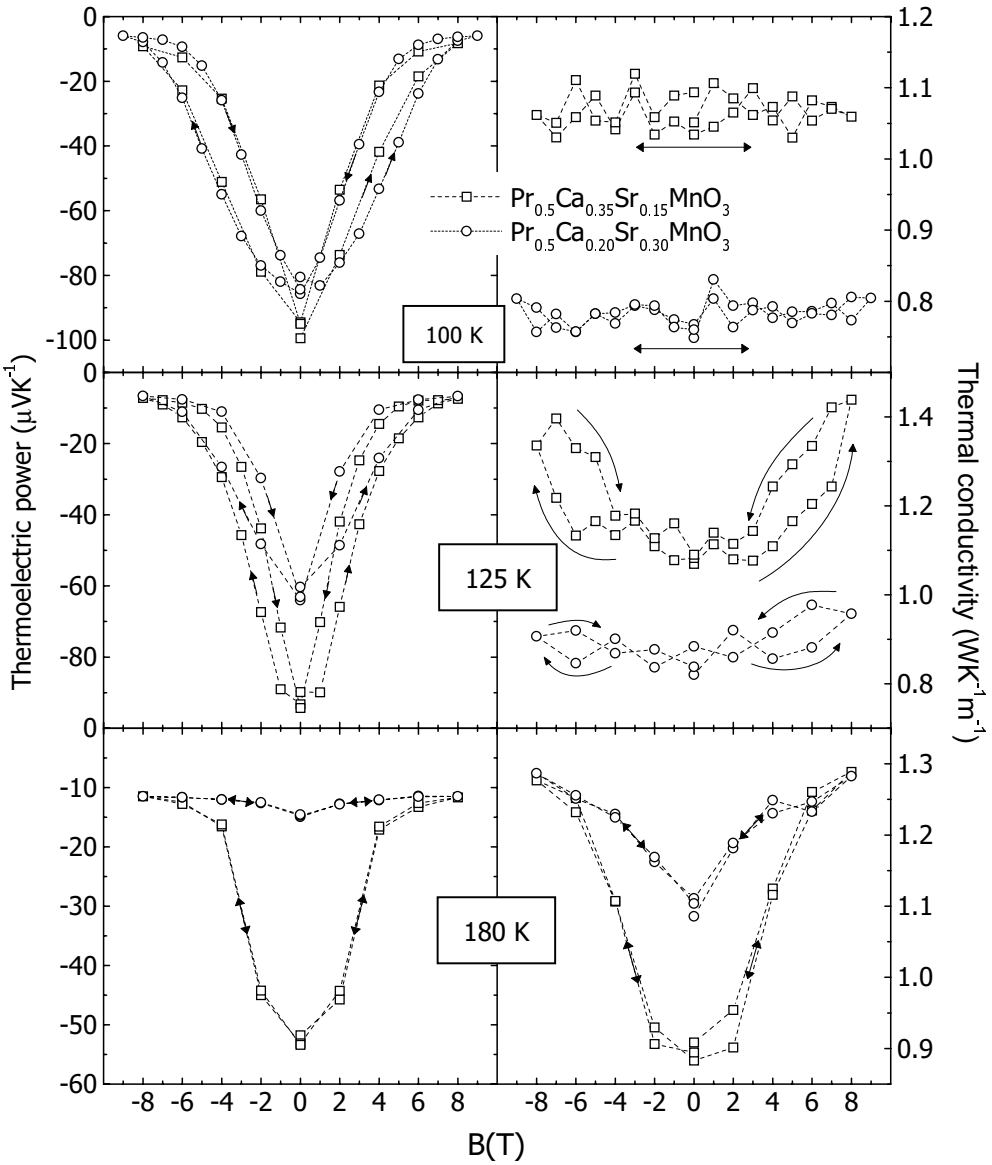

Figure 10. Thermoelectric power α (left-hand panels) and the thermal conductivity λ (right-hand panels) in a sweeping magnetic field up to 9 T, taken at several constant temperatures for $x = 0.15$ (squares) and $x = 0.3$ (circles).

magnetic measurements, the accompanying crystallographic change need not be seen in the neutron diffraction experiment. Similar problems may appear in the opposite case when the spontaneous magnetic moment of very small FM inclusions is to be determined by neutron diffraction. Finally, as indicated above, NMR can fail in the observation of the signal from fast relaxing FM domains which may be identified again with small (quasi-superparamagnetic) particles or inclusions. The comparison shown in figure 12 for the $x = 0.3$ case represents a good illustration.

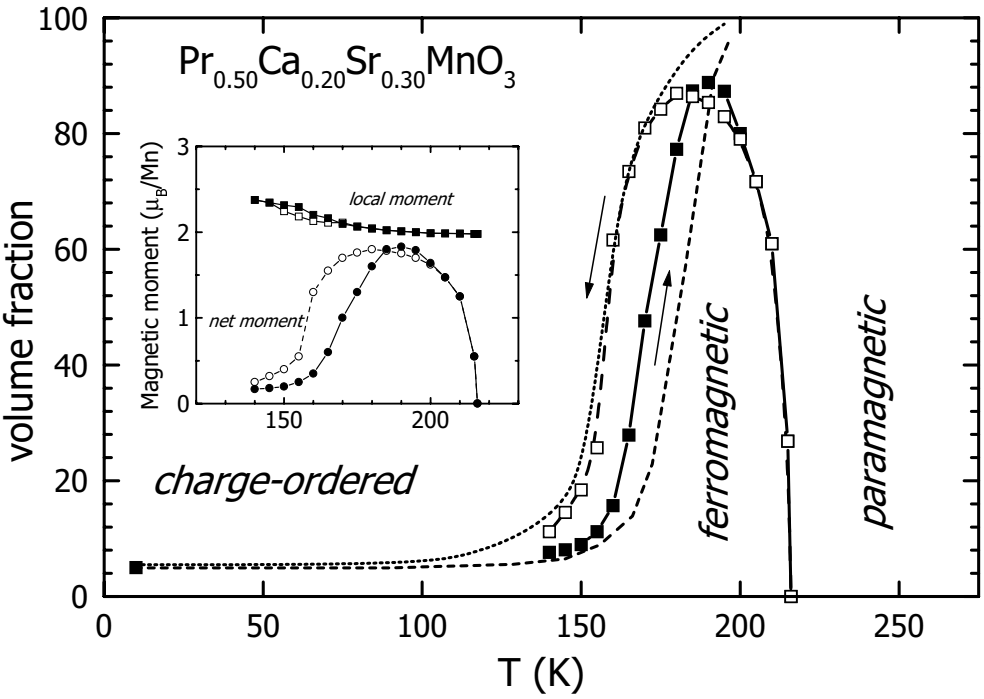

Figure 11. Phase diagram of $Pr_{0.5}Ca_{0.2}Sr_{0.3}MnO_3$. The dotted curves show the distribution among the pseudocubic and tetragonally distorted structures, for cooling and warming (see also figure 1(b)). The open and full symbols relate to the FM volume ($B + A$) deduced from the observed net magnetization and the NMR data on local moments which are both displayed in the inset.

All these observations lead to the conclusion that the FM B phase appears in a form of very fine domains as a result of phase separation and these domains gradually grow when the temperature is lowered. As shown in [25] the appearance of phase B at T_C is preceded by formation of mutually competing CO (or Jahn–Teller) and superparamagnetic clusters. At $T \rightarrow T_C$ the latter ones become dominant, grow up and, finally, they may be stabilized due to the occupation by e_g electrons of certain extended (itinerant or molecular) orbitals within the clusters and the corresponding promotion of the double-exchange (DE) interactions, in accordance with the ideas of Goodenough and coworkers [3, 5, 29]. The experimentally found T_C should then correspond to T_C' according to the notation introduced in [29]. The formation of clusters with delocalized electrons is related to the trapping out of some of the mobile polaronic carriers which separate the material into small FM domains with metallic-like electrical conductivity, embedded in a PM insulating phase. The B-phase clusters are probably very small, their size (and shape) being controlled by Coulomb forces originating from the assumedly different electronic charge densities of both coexisting phases [9, 30]. On the other hand, segregation of the B phase and the growth of its volume on cooling is expected to support the CO cluster formation in the coexisting PM phase which at $T_{co} = 200$ K starts a first-order transition to the tetragonally contracted CO phase. But, interestingly, this alone is not sufficient to stop the growth of the FM phase volume (figure 11) which continues to fill in the remaining quasicubic phase until the antiferromagnetism below T_N^C quickly destroys both the ferromagnetism and the quasicubic phase.

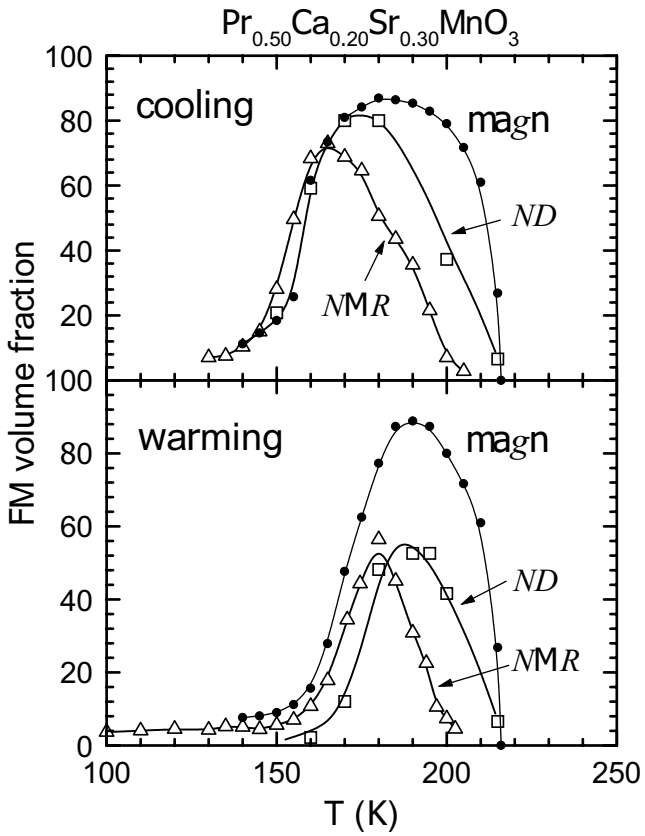

Figure 12. The FM phase volume seen in independent experiments—magnetic, neutron diffraction and NMR. The calibration point for NMR is $T = 165$ K at cooling. The neutron diffraction data were determined by a re-evaluation of the magnetic neutron diffraction intensities in terms of volume fractions, using the local moments in the inset of figure 11.

The continuing tendency for the segregation of the FM phase manifests itself mainly in the development of the minority phase A, probably at the border of the newly formed CO phase. As shown in figure 3 the NMR frequency F_{A_1} depends very weakly on temperature for $T_N < T < T_{co}$ similarly to F_B, only its value is slightly higher. This indicates that even the origin of the ferromagnetism A_1 might be similar to that of B, i.e. the FM clusters locally stabilized by DE interactions of electrons moving in some spatially extended orbitals within the clusters. Only the character of these orbitals is probably different, for example due to the geometrically and/or the physically differentiated background. On the other hand, simultaneously with the decline of the FM phase B in the vicinity of T_N, both F_{A_1} and F_{A_2} begin to grow towards low temperatures in a way which is very similar to the temperature dependence of the NMR frequency observed in the FM metallic-like manganites [27, 31, 32].

The A-type ferromagnetism only is detected for $x = 0.15$. The corresponding T_C was determined as 195 ± 5 K which is distinctly below the critical temperature $T_{co} = 210$ K at which the CO phase first appears. In spite of the presence of FM clusters above T_C [25] and the fact that the fraction volume of the pseudocubic phase at ∼190 K is still 80% (figure 1), no B-type ferromagnetism appears. The possible explanation for this could be sought in the characteristics of possible clusters. While for $x = 0.3$ the higher concentration

of large Sr ions effectively increases the local tolerance factor t and thus could create local extended e_g electronic states, such states are probably considerably restricted in both their extension and stability for $x = 0.15$. Moreover, due to the smaller concentration of Sr ions the tolerance factor t will then also be diminished which decreases the transfer integral for e_g electrons and weakens the DE interactions. Hence, while for $x = 0.3$ the originally superparamagnetic clusters become static FM clusters with possibly different e_g concentration (electronic phase separation), the superparamagnetic clusters remain dynamic in $x = 0.15$ and stable FM slabs (or clusters) then appear only when in contact with the tetragonally deformed CO phase, possibly as a regular accompanying effect during the development of this new phase. The arguments pointing to the intrinsic character of the formation of certain defects during transformation to the CO phase are included, for example, in [20, 33, 34].

In figure 13(a) three basic types of defects in a charge and orbitally ordered 1:1 Mn^{3+}/Mn^{4+} perovskite are shown, i.e. discommensuration, dislocation and antiphase boundary. All of them violate the regular alternation of Mn^{3+} orbitals and disturb the magnetic order at Mn^{3+} sites while the ordering in the Mn^{4+} sublattice is not influenced. Both the dislocations and antiphase boundaries appear unstable due to the unfavourable orientation of some e_g orbitals and may give rise to other AFM phases, for example the C- type or A-type arrangements. We believe that the parasitic FM regions giving rise to the NMR signals A_1 and A_2 may also be of this origin. A more detailed analysis shows that the antiphase boundary should be preferred from the point of view of stability. Possible stacking of the CO and FM phases is shown in figure 13(b), satisfying the requirements of a minimization of elastic stresses and magnetic frustration at the interphase.

In order to complete our picture we shall now discuss the behaviour of both materials under the influence of an applied magnetic field. Although the direct observations by means of neutron diffraction or NMR has not been at our disposal, some basic conclusions can be drawn even in an indirect way from magnetization and transport measurements performed in a strong magnetic field. As in many 1:1 Mn^{3+}/Mn^{4+} perovskites with the CO CE-type AFM structure at low temperature [35], the metallic DE FM state is expected to be induced by a strong magnetic field. From this point of view, the non-standard forms of ferromagnetism A, B can be regarded as nuclei or some kind of precursors of the final bulk FM state. This is really confirmed by a steady increase of the overall magnetic moment in an increasing magnetic field, reaching in 5 T values which refer to $M(T)$ curves in figure 5. A comparison of both compositions for the values at $T/T_C \sim 0.75$ with the theoretical Weiss molecular field curve, reveals that not only the volume of the FM phase has increased under the influence of magnetic field but also the original anomalously low magnetic moment per Mn ion ($\sim 2\ \mu_B$) has approached its expected value that would correspond to $\sim 3.5\ \mu_B$ for $T \to 0$. In parallel, both the thermopower α and the thermal conductivity λ increase to their saturated values, which bears witness to the metallic character of the high-field FM phase. The behaviour of the electrical resistivity $\rho(T)$ need not to be taken as decisive when exhibiting a negative derivative $\mathrm{d}\rho/\mathrm{d}T$ below T_C in both compositions because of the possible influence of intergranular barriers as is often the case in ceramic samples. Yet the $\rho(T)$ curves at 5 T are far from expressing a thermal activation as $-\mathrm{d}\rho/\mathrm{d}T$ is decreasing below T_C and, in particular for $x = 0.3$, it has a tendency to approach zero (figure 5).

The bulk FM state is definitely induced at temperatures $T \geqslant T_N$. Even though the magnetic field extends the FM region a little towards lower temperatures, at temperatures lower than about 20–30 K below T_N the magnetic field of 5 T is not sufficient to drive the transition from the CO tetragonally deformed structure stabilized by the CE-type AFM order to the pseudocubic FM phase and the conversion cannot be fully realized. Yet a partial effect still exists and beside an increase of the magnetic moment it manifests itself by changing the character of

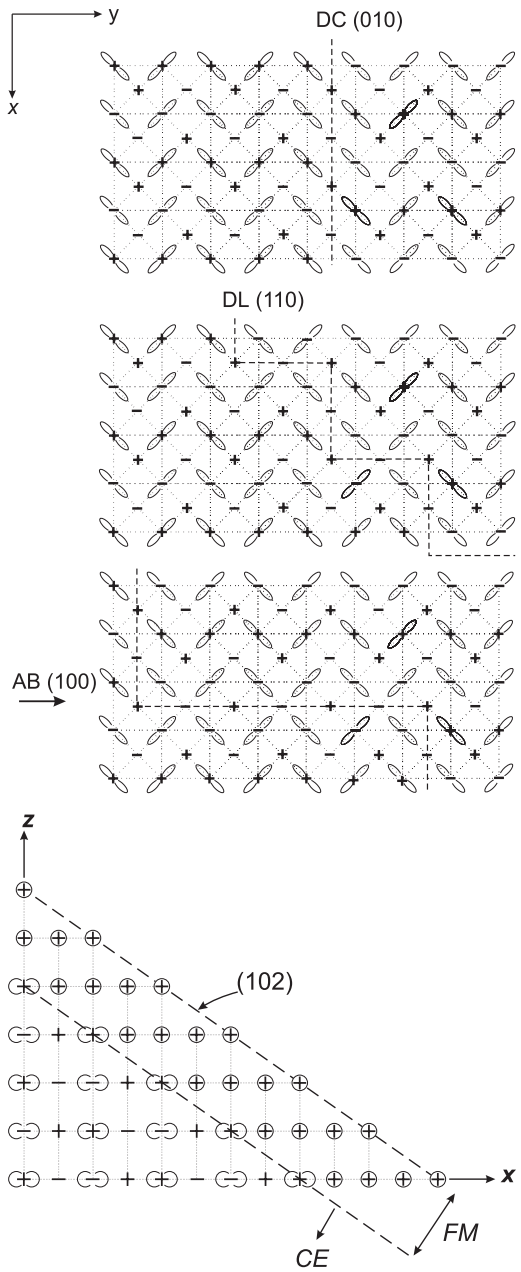

Figure 13. (a) Orbital defects in the 1:1 Mn^{3+}/Mn^{4+} ordered phases shown in the (001) plane of the *Pbnm* perovskite cell—discommensuration (DC), dislocation (DL) and the antiphase boundary (AB). The Mn^{3+} sites are depicted with lobes, the Mn^{4+} sites by spheres. The + and − signs show the spin orientation in the CE-type AFM state; successive layers possess identical orbital arrangement but opposite spins. It appears that, unlike the Mn^{4+} sublattice, the long-range coherence of the Mn^{3+} magnetic order is always lost at the orbital defect, which may result in an apparent decrease of the Mn^{3+} moments when determined by neutron diffraction. (b) Possible stacking of the CO and FM phases viewed along the *y*-direction of the *Pbnm* cell. The CO CE-type AFM phase is significantly contracted along the *z*-axis while the FM phase is pseudocubic.

the $\rho(T)$ curves in the low-temperature range below $\approx$100 K (figure 5); see also [36]. The resistivity saturates there and becomes temperature independent. High values indicate that the conduction due to the percolation effect between small metal-like FM domains would be a more appropriate explanation than metallic conductivity in the bulk. The role of the magnetic field should then consist in an alignment of the magnetization in separate domains [9] and in increasing their volume and/or number. This conclusion is supported by the different behaviour of α and λ in the magnetic field at low temperatures (figure 10). While the thermopower grows and saturates in fields from 5 T to 9 T, the thermal conductivity remains practically constant in contrast to higher temperatures at which the complete FM order appears. The behaviour of α at $T \leqslant 100$ K agrees with the findings of Kim *et al* [37], who showed that in contrast to λ the thermopower may exhibit a metal-like behaviour even at the percolation threshold. Let us also note that the lower resistivity at $T < 100$ K for $x = 0.15$ obviously corresponds to a larger volume of parasitic pseudocubic domains (FM or magnetically disordered) surviving to low temperatures or becoming newly formed in the magnetic field from some spins which are loosely bound to the AFM phase [25].

Finally, the alignment of magnetic moments in weak fields (up to 1 T) may be the cause of an appreciable magnetoresistance provided that the FM phase has reached the percolation limit. The increase of the electrical conductivity is then the result of easier electric transport along the magnetically ordered path. This is expected to be the case with $x = 0.3$ at temperatures between $\approx$110 K and 180 K. On the other hand, the magnetoresistance in higher magnetic fields is connected with the phase transition induced by the magnetic field. Here the volume of the FM phase is increased which enables the transport. As a typical example see the magnetoresistance of $x = 0.15$ between $\sim$140 K and 180 K (figure 7).

5. Conclusion

Using a complex experimental investigation, we have been able to improve the detailed picture of the course of phase transitions in typical compositions of the series $Pr_{0.5}Ca_{0.5-x}Sr_xMnO_3$ ($x = 0.15, 0.3$). The background is formed by, in principle, a first-order structural transition between the high-temperature pseudocubic and the low-temperature tetragonally deformed, 1:1 Mn^{3+}/Mn^{4+} ordered phases. The PM to FM transition realized within the pseudocubic phase for $x = 0.3$ proceeds by stabilization of superparamagnetic clusters and is accompanied by an electronic phase separation in which a partial delocalization of e_g electrons within some extended orbitals inside the clusters takes place. Such a type of ferromagnetism was reported in some CMR materials with an Mn^{3+}/Mn^{4+} ratio close to 2:1 [5, 29]. The minority ferromagnetism, detected in both compositions in parallel with the CO phase, was ascribed to the existence of specific defects (probably the antiphase boundaries). The magnetic field of 5 T transforms both materials to a state close to bulk ferromagnetism provided that the temperature is high enough (>140 K). At lower temperatures higher fields would be needed, while 5 T makes only percolative effects in the electrical transport.

Acknowledgments

The research was performed under a support of the Grant Agency of the Czech Republic (grant No 202/99/0413). Experiments at the Hahn-Meitner-Institut in Berlin were supported by the European Commission through the Human Capital and Mobility (PECO) programme 'Access to large-scale facilities'.

References

[1] von Helmholt R, Wecker J, Holzapfel B, Shulz L and Sammer K 1993 *Phys. Rev. Lett.* **71** 2331
[2] Jin S, Tiefel T H, McCormack M, Fastnacht R A, Ramesh R and Chen L H 1994 *Science* **264** 413
[3] Goodenough J B 1997 *J. Appl. Phys.* **81** 5330
[4] Ramirez A P, Cheong S-W and Shiffer P 1997 *J. Appl. Phys.* **81** 5337
[5] Goodenough J B 1999 *Aust. J. Phys.* **52** 155
[6] Tomioka Y, Asamitsu A, Moritomo Y, Kuwahara H and Tokura Y 1995 *Phys. Rev. Lett.* **74** 5108
[7] Kuwahara H, Tomioka Y, Asamitsu A, Moritomo Y and Tokura Y 1995 *Science* **270** 961
[8] Tokura Y, Kuwahara H, Moritomo Y, Tomioka Y and Asamitsu A 1996 *Phys. Rev. Lett.* **76** 3184
[9] Moreo A, Yunoki S and Dagotto E 1999 *Science* **283** 2034 and references therein
[10] Hennion M *et al* 1998 *Phys. Rev. Lett.* **81** 1957
[11] Allodi G, de Renzi R, Licci F and Pieper M W 1998 *Phys. Rev. Lett.* **81** 4736
[12] de Teresa J M *et al* 1997 *Nature* **386** 256
[13] Uehara M, Mori S, Cher C H and Cheong S-W 1999 *Nature* **399** 560
[14] Fath M *et al* 1999 *Science* **285** 1540
[15] Moreo A, Mayr M, Feiguin A, Yunoki S and Dagotto E 2000 *Phys. Rev. Lett.* **84** 5568
[16] Heffner R H *et al* 2000 *Phys. Rev. Lett.* **85** 3285
[17] Chechersky V, Nath A, Michel C,Hervieu M, Ghosh K and Greene R L 2000 *Phys. Rev.* B **62** 5316
[18] Papavassiliou G, Fardis M, Belesi M, Maris T G, Kallias G, Pissas M, Niarchos D, Dimitropoulos C and Dolinsek J 2000 *Phys. Rev. Lett.* **84** 761
[19] Savosta M M and Novak P 2000 *Phys. Rev. Lett.* submitted
[20] Jirák Z, Damay F, Hervieu M, Martin C, Maignan A, Raveau B, André G and Bourée F 2000 *Phys. Rev.* B **61** 1181
[21] Damay F, Martin C, Hervieu M, Maignan A, Raveau B, André G and Bourée F 1998 *J. Magn. Magn. Mater.* **184** 71
[22] Jirák Z *et al* 2001 *J. Appl. Phys.* **89** 7404
[23] Wolfman J, Simon Ch, Hervieu M, Maignan A and Raveau B 1996 *J. Solid State Chem.* **223** 413
[24] Damay F, Martin C, Maignan A, Hervieu M, Raveau B, Jirák Z, André G and Bourée F 1999 *Chem. Mater.* **11** 536
[25] Krupička S, Maryško M, Jirák Z and Hejtmánek J 1999 *J. Magn. Magn. Mater.* **206** 45
[26] Savosta M M, Karnachev A S, Krupička S, Hejtmánek J, Jirák Z, Maryško M and Novák P 2000 *Phys. Rev.* B **62** 545
[27] Savosta M M, Borodin V A and Novák P 1999 *Phys. Rev.* B **59** 8778
[28] Nagaev E L 1998 *Phys. Rev.* B **58** 2415
[29] Archibald W, Zhou J S and Goodenough J B 1996 *Phys. Rev.* B **53** 1445
[30] Nagaev E L 1994 *Phys. Status Solidi* b **186** 9 and references therein
[31] Savosta M M, Borodin V A, Novák P, Jirák Z, Hejtmánek J and Maryško M 1998 *Phys. Rev.* B **57** 13 379
[32] Savosta M M, Hejtmánek J, Jirák Z, Maryško M, Novák P, Tomioka Y and Tokura Y 2000 *Phys. Rev.* B **61** 6896
[33] Chen C H and Cheong S-W 1996 *Phys. Rev. Lett.* **76** 4042
[34] Radaelli P G, Cox D E, Marezio M and Cheong S-W 1997 *Phys. Rev.* B **55** 3015
[35] Tokunaga M, Miuro N, Tomioka Y and Tokura Y 1998 *Phys. Rev.* B **57** 5259
[36] Chang C W, Huang C Y, Dai M F and Lin J G 2000 *J. Phys.: Condens. Matter* **12** 9425
[37] Kim K H, Uehara M, Hess C, Sharma P A and Cheong S-W 2000 *Phys. Rev. Lett.* **84** 2961